Appl. Phys. B (2015) 119:55–64
DOI 10.1007/s00340-015-6008-1

Applied Physics B
Lasers and Optics

Novel utilisation of a circular multi-reflection cell applied to materials ageing experiments

D. A. Knox · A. K. King · E. D. McNaghten · S. J. Brooks · P. A. Martin · S. M. Pimblott

Received: 30 October 2014 / Accepted: 9 January 2015 / Published online: 8 February 2015

Abstract We report on the novel utilisation of a circular multi-reflection (CMR) cell applied to materials ageing experiments. This enabled trace gas detection within a narrow interfacial region located between two sample materials and remotely interrogated with near-infrared sources combined with fibre-optic coupling. Tunable diode laser absorption spectroscopy was used to detect water vapour and carbon dioxide at wavelengths near 1,358 and 2,004 nm, respectively, with corresponding detection limits of 7 and 1,139 ppm m $Hz^{-0.5}$. The minimum detectable absorption was estimated to be 2.82×10^{-3} over a 1-s average. In addition, broadband absorption spectroscopy was carried out for the detection of acetic acid, using a superluminescent light emitting diode centred around 1,430 nm. The 69 cm measurement pathlength was limited by poor manufacturing tolerances of the spherical CMR mirrors and the consequent difficulty of collecting all the cell output light.

1 Introduction

Materials ageing studies often require the capability to monitor in situ chemical changes which occur within the system under investigation via non-invasive techniques, in order to avoid perturbing the environment within the sample vessel. Absorption spectroscopy offers a convenient means of achieving this aim. This applies to both the ageing of individual materials in isolation and the study of the interactions between combinations of materials. The ageing of a wide range of active materials (metals, polymers, ceramics, etc.) may be studied in 'real time' at ambient temperatures or under accelerated ageing conditions [1] where temperatures are elevated, typically by a few tens of degrees, in order to increase the rates of ageing reactions without significantly altering the nature of the reactions occurring. Under the latter set of conditions, the requirement for the ageing experiment to remain at elevated temperature for extended periods of time may impose restrictions on the nature of the diagnostics which may be used to study it.

A key component of this research was the analysis of gaseous atmospheres within a material ageing experiment, because evolved gas composition can be indicative of the chemical changes occurring in the condensed phases. If possible, it is desirable to analyse the gas as close as possible to the point at which it is evolved. In the case of a multi-material experiment (MME), the interfacial region between pairs of materials is therefore of interest. Hence, there is a requirement for diagnostic techniques which are capable of characterising/quantifying gas-phase species within the restricted environments.

A typical MME would consist of two samples, separated by 1–5 mm, in a hermetically sealed vessel, possibly held within a temperature-controlled chamber. Hence, the interfacial region would constitute a cylindrical space, the diameter of which is significantly greater than its height. Figure 1 presents a schematic illustration of the typical location of samples within an MME arrangement.

D. A. Knox (✉) · A. K. King · E. D. McNaghten · S. J. Brooks
AWE, Aldermaston, Reading RG7 4PR, UK
e-mail: David.Knox@awe.co.uk

P. A. Martin
School of Chemical Engineering and Analytical Science, University of Manchester, Oxford Road, Manchester M13 9PL, UK

S. M. Pimblott
School of Chemistry, University of Manchester, Oxford Road, Manchester M13 9PL, UK

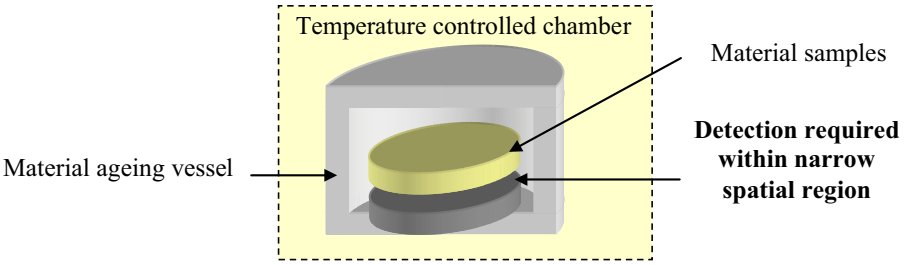

Fig. 1 Typical MME arrangement

In 1994, Thoma et al. published the first report of a novel class of multi-pass optical cell, usually termed a circular multi-reflection (CMR) cell. As the name implies, such a cell is characterised by all the points of reflection lying around the circumference of a circle. This arrangement provides planar reflection geometry, as illustrated in Fig. 2.

This was followed by reports of a number of similar cells by various research groups [2–8]. Details of these systems are summarised in Table 1. As Table 1 indicates, CMR cells have, in general, been constructed with pathlengths in the one to four metre region and typical diameters of around ten centimetres. A variety of different mirror types have been used (cylindrical, spherical and toroidal), formed from either turned and polished metal, or coated silica substrates. It is notable that, to date, only CMR systems optimised for use in either the mid-infrared (mid-IR) or visible/ultraviolet (UV) regions have been reported.

Whilst the pathlength available in CMR cells is less than that available from conventional multi-pass cells such as the Herriott or White cells [9–11], the overall dimensions, coupled with the aforementioned optical planarity, suggest that a CMR arrangement would be well suited to the analysis of the atmosphere contained within the interfacial region between two cylindrical samples of materials. This concept is illustrated in Fig. 3. If an accelerated ageing experiment were required, it would be necessary to employ optical fibres to transport light to and from the CMR system, as it would be impractical to place both source and detector within a temperature-controlled chamber. This, in turn, would suggest the necessity of working in the near-IR band, due to the considerably greater maturity of near-IR fibre technology. The disadvantage incurred by operating in the near-IR region compared to the mid-IR is the well-known reduction in absorption cross sections compared to the mid-IR.

In order to implement this design, we have constructed and characterised a novel fibre-coupled CMR system, which was optimised for the near-IR region. This cell was housed within a specially adapted trial vessel that was designed to facilitate the analysis of interface conditions. Calibration of the system for the detection of three different analyte molecules was undertaken. The analytes comprised carbon dioxide (CO_2), water (H_2O) and acetic acid

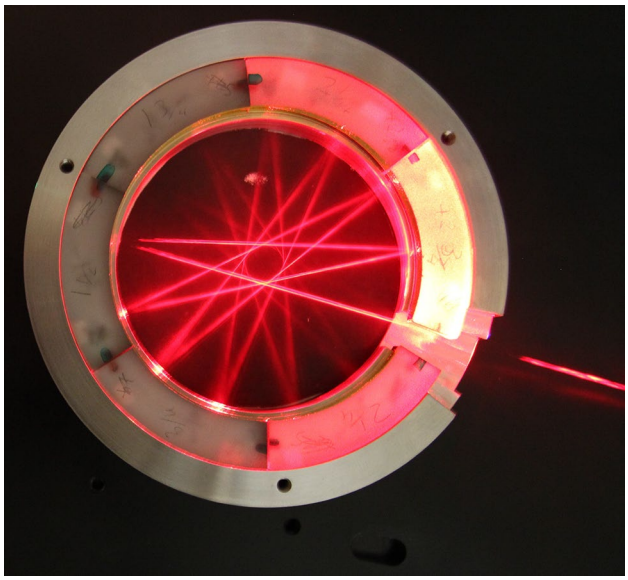

Fig. 2 Circular multi-reflection cell, which demonstrates a 13-pass configuration. 633-nm alignment beam visualised using liquid nitrogen vapour

(CH_3CO_2H)—a representative volatile organic compound (VOC). The target detection range was 100–10,000 ppm, the gases being evolved from samples typically 1.5 cm thick and 6.0 cm diameter. Detection of CO_2 and H_2O involved the use of tunable diode laser absorption spectroscopy (TDLAS) and was detected using a photoreceiver, and for acetic acid, broadband absorption spectroscopy (BBAS) was employed which made use of a superluminescent light emitting diode (SLED) source and an optical spectrum analyser (OSA). In all three cases, calibrated reference samples were used to determine the sensitivity for the analyte of interest.

In this paper, we describe the design and construction of a CMR optical cell and its incorporation into an MME arrangement using fibre-coupled mounted optics. This will be followed by a description of the experimental arrangement used for the spectroscopic techniques (TDLAS and BBAS) and details of their subsequent processing and analysis. Calibration of the system against the target analytes and characterisation of system noise will then follow.

Table 1 CMR cells reported in the literature

References	Year published	Mirrors		Material	Diameter (cm)	Optical path length (cm)	Cell volume (cm^3)	Radiation source wavelength (λ)	Target analyte
[2]	1994	8	Cyl	Coated SS	10	86	Not stated	257 nm (UV)	Ozone
[3]	2005	?	Cyl	Coated Al	16	288	Not stated	488 nm (UV)	NO_2
[4]	2007	6	Cyl	Not stated	16	458	25	~533 nm (visible)	n/a
[5]	2010	1	Sph	Polished Al	6	105	78	4,167–4,380 nm (mid-IR)	CO_2
[6]	2012	6	Sph	Au-coated glass	10	310	24	4,476–4,456 nm (mid-IR)	$^{13}CO_2/N_2O$
[7]	2013	1	Tor	Turned Cu, Au coated	8	216	40	4,329 nm (mid-IR)	CO_2
[8]	2014	1	Tor	Turned Cu, Au coated	8	408	40	4,329 nm (mid-IR)	$^{13}CO_2/^{12}CO_2$

Cyl cylindrical, *Sph* spherical, *Tor* toroidal, *SS* stainless steel

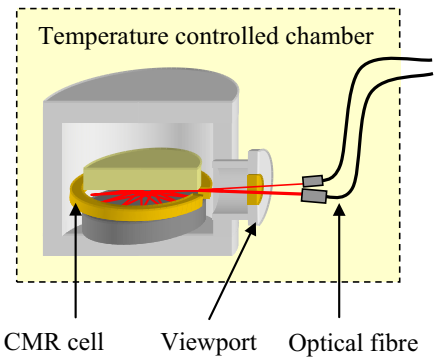

Fig. 3 Proposed use of a CMR cell to interrogate the narrow region formed between two coupons

2 Experimental

2.1 Design and construction

A CMR mirror design similar to that described by Manninen et al. [6] was used. This utilised six gold-coated spherical mirrors, with a radius of curvature of 3.250 (±0.005) cm, arranged in a circular pattern about their mutual focal point. The six mirrors, each of 0.600 (±0.005) cm height and 1.000 (±0.005) cm depth, formed 57.5° (±10′) segments of the circular configuration, leaving a 15.0° aperture (0.85 cm wide) for the optical radiation to interrogate the CMR cell. The cylindrical volume in which the beam passed was estimated to be 13 cm^3 [π × (radius of curvature 3.25 cm)^2 × (radiation beam waist 0.40 cm)]. The mirrors were supplied by Envin Scientific Ltd (UK).

A bespoke holder was designed to secure the mirrors in place, as well as accommodate the two material samples. The holder comprised three components: a base, lid and locator wedge, as illustrated in Fig. 4. The base provided a flat surface on which the six mirrors were mounted and a lower well to accommodate the bottom sample. A 26° aperture for laser interrogation was provided in the plane of the mirrors; this was wider than the 15° mirror aperture to permit larger interrogation angles to be achieved, if required. The lid was used to secure the mirrors in place via M3 tapped holes located above each mirror, and Nylon-tipped set screws. Three additional holes were located around the lid circumference in order to secure the lid to the base, again using M3 bolts. The lid featured a circular aperture to allow the upper material sample to be

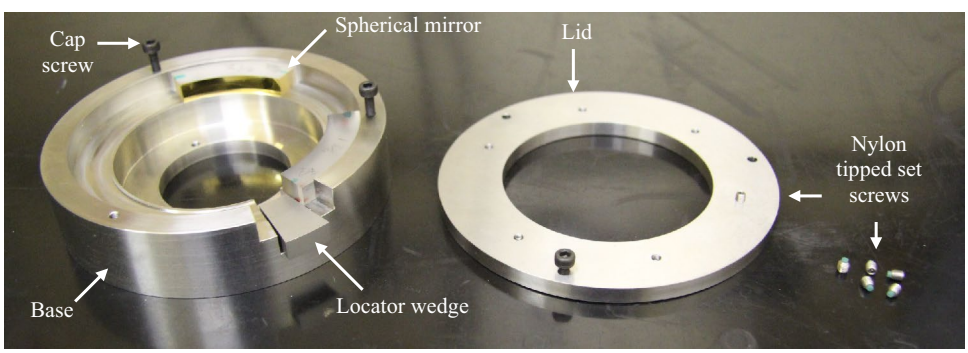

Fig. 4 CMR holder which comprised a base, lid and locator wedge

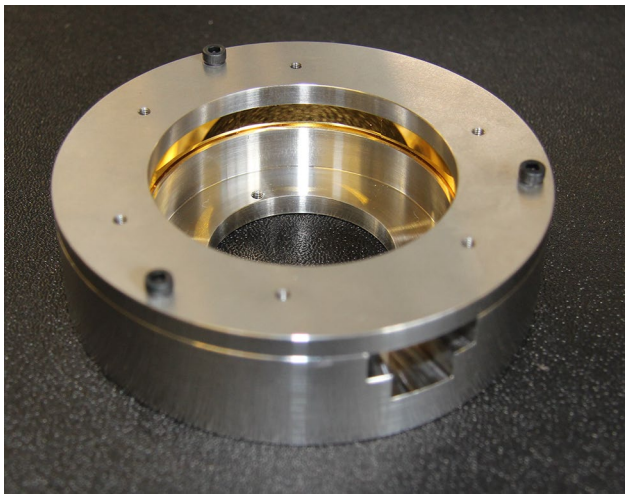

Fig. 5 Complete CMR cell

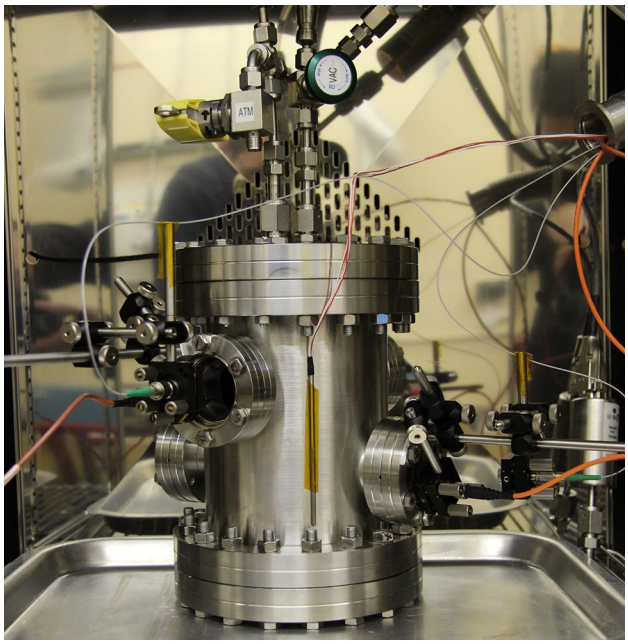

Fig. 6 CMR vessel with mounted optics, pictured here within the temperature-controlled chamber. Addition viewports incorporated for future experimental capability

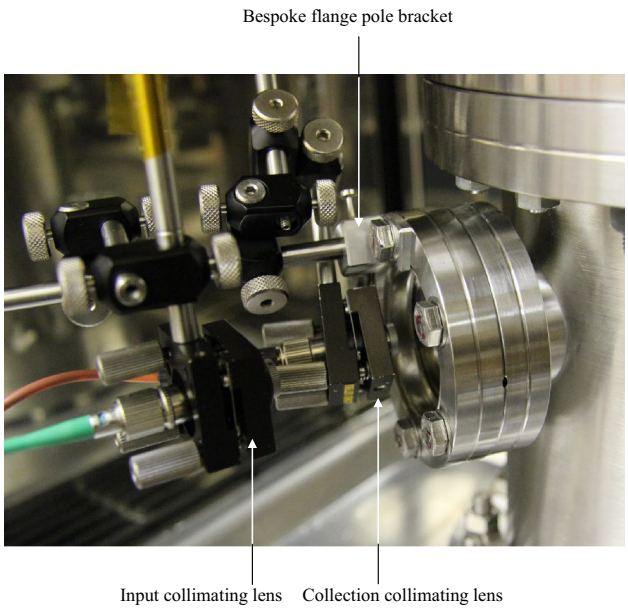

Fig. 7 Flange-mounted optics were required to interrogate the CMR cell

suspended above the optical beam path. The final component of the CMR holder was a 15° locator wedge, which was used to retain the mirrors in place through a 'keystone' style interference fit. The wedge was located in a recess below the plane of the mirrors, standing slightly proud of the recess, so as to make contact with the mirror edges whilst still allowing optical radiation to enter/exit the cell. All holder components were manufactured in stainless steel by Duckworth & Kent Ltd (UK). Figure 5 shows the fully assembled CMR cell.

An evacuatable materials ageing vessel (shown in Fig. 6) was manufactured which could accommodate the CMR cell and material samples. This incorporated a 2 ¾″ (7 cm) viewport to allow the near-IR radiation to be coupled in and out of the CMR cell. Mounting points for the CMR cell were located on the base of the vessel, and connections for monitoring the pressure were located on the lid. The temperature and pressure within the cell were monitored using a platinum resistance thermometer (PRT) and pressure transducer, respectively. Two additional ports for evacuating the vessel and backfilling with gas were also provided. The cell was evacuated using a rotary vane vacuum pump (Edwards). For the purposes of materials ageing experiments, the vessel was placed in a temperature-controlled chamber (LTE Scientific Ltd).

Two single-mode optical fibres were used with collimators to couple the near-IR radiation into and out of the vessel, via the viewports mentioned above. These were maintained in the correct position and alignment by adjustable mounts attached to a short post affixed to the outside of the viewport using a bespoke bracket as shown in Fig. 7. By varying the positions of the two collimators, a variety of different optical paths through the CMR cell could be accessed, with up to thirteen reflections possible. Initial evaluation of the system showed that a nine-pass configuration gave the best compromise between sensitivity and stability of the system. This equated to a pathlength of 58 cm between the CMR mirrors, with an additional 11 cm of

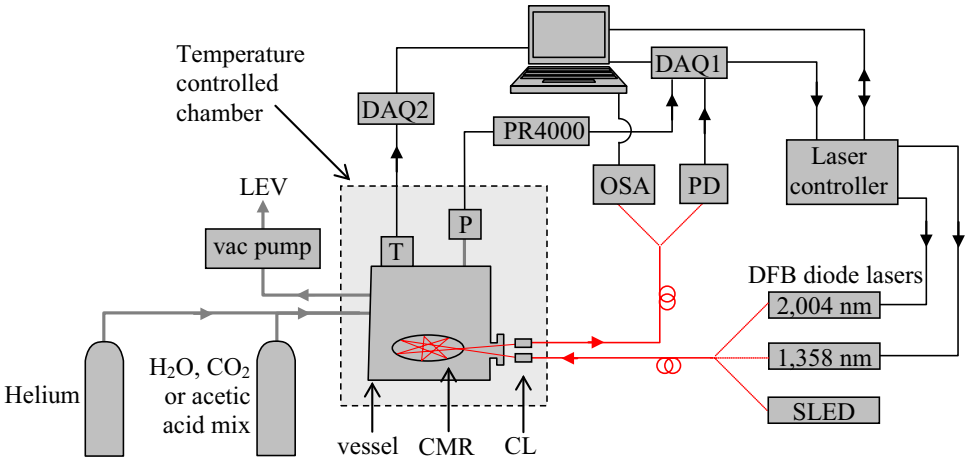

Fig. 8 Experimental arrangement. *CMR* circular multi-reflection cell, *DAQ* data acquisition, *DFB* distributed feedback diode laser, *CL* collimating lens, *LEV* local exhaust ventilation, *OSA* optical spectrum analyser, *P* pressure transducer, *PD* photodiode, *T* Pt100 temperature probe

pathlength between the mirrors and the viewport. Thus, the total internal pathlength was 69 cm. The vessel was custom built by Kurt J. Lesker Ltd (UK), optical fibres and mounting components being obtained from Thorlabs GmbH and collimators from Micro Laser Systems Inc. (USA).

The apparatus for the TDLAS experiments consisted of two distributed feedback (DFB) diode lasers, supplied by Nanoplus (Germany), the wavelength of which was centred around 1,358 and 2,004 nm, to facilitate the detection of H_2O and CO_2, respectively. A laser diode controller (Thorlabs, PRO 8000) was used to vary the temperature and current applied to the diodes. The transmitted optical radiation was fibre-coupled out of the vessel and directed onto an extended-λ InGaAs photoreceiver (New Focus, Model 2034).

The TDLAS experiment was controlled by a PC which interacted with the diode controller and photoreceiver via a data acquisition card (National Instruments PCI-6259) and associated interface box (National Instruments BNC-2110). A LabVIEW program was used to control the operation of the system and to automate data collection. The PC was also used to log pressure and temperature readings using a Baratron pressure transducer (MKS), connected to a digital readout (MKS), and a Pt100 PRT probe (RS Components), respectively. This arrangement is shown in Fig. 8.

A PC (Windows 7, 64-bit) was used to control, collect and process the experimental data using a bespoke National Instruments LabVIEW 2013 program. TDLAS spectra were recorded at a rate of 10 Hz. Each spectrum consisted of two periods during which the diode laser output was swept over the wavelength region of interest by varying the diode voltage, interspersed with two periods during which the diode was biased into its dark region and no light was generated. These latter two periods were necessary to obtain an accurate baseline. Spectra were digitised at a rate of 100 kHz, and thus each spectrum comprised 10,000 data points. For H_2O, the laser was scanned over a range of 1,356.55–1,357.26 nm, and for CO_2, 2,003.15–2,004.61 nm. For each measurement, 100 spectra were summed and the averaged spectrum was then analysed using a LabVIEW program, which used non-linear least squares fitting to deconvolute the spectrum into a polynomial baseline and a series of pseudo-Voigt functions (linear combinations of Lorentzian and Gaussian profiles with independently variable coefficients of each). The program also calculated the target analyte volume mixing ratio (ppm), derived from the area under the fitted peak, the temperature/pressure of the vessel and the relevant calibration data.

Broadband absorption spectroscopy was carried out using a fibre-coupled SLED source, supplied by DenseLight Semiconductors Pte Ltd (Singapore), and an OSA, supplied by Thorlabs. The SLED radiation exhibited a Gaussian emission profile centred around 1,430 nm, with a full-width at half-maximum (FWHM) of around 40 nm. BBAS spectra were recorded at a resolution of 38 pm (high resolution, high sensitivity mode), which limited the mirror sweep speed of the interferometer, resulting in a collection and processing time of 11 s (0.091 Hz) per spectrum. As before, 100 spectra were summed and averaged. Absorbance spectra were obtained by ratiometric comparison with a reference spectrum obtained from the empty vessel. These usually demonstrated significant baseline variations which were subsequently removed by least squares fitting of an appropriate polynomial. A low-pass Butterworth filter was used to remove high-frequency noise from the resulting trace.

2.2 Calibration

The CMR vessel was calibrated for the detection of three analytes (H_2O, CO_2 and acetic acid). For H_2O and CO_2, the calibration involved the use of a certified gas standard which was diluted to various degrees, with spectra recorded

Table 2 Target analyte with their details from the HITRAN database [12]

Species	Line position (cm^{-1})	Band	Line strength at 296 K [$cm^{-1}/(mol/cm^{-2})$]
$H_2^{16}O$	7,368.40788	$\nu_1 + \nu_3$	6.979×10^{-21}
$^{12}C^{16}O_2$	4,989.971515	$\nu_1 + 2\nu_2 + \nu_3$	1.287×10^{-21}

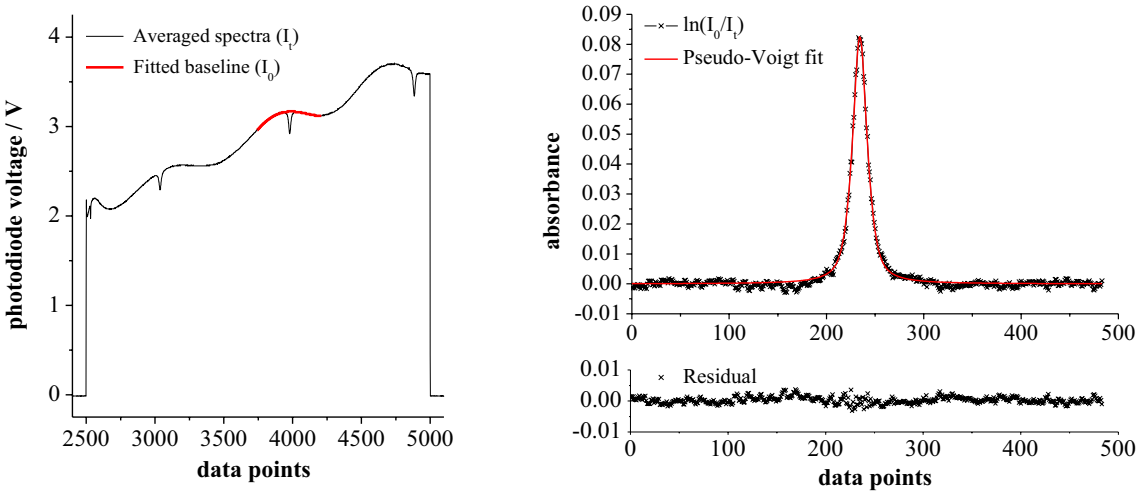

Fig. 9 A typical TDLAS spectrum and peak fit for CO_2 in helium, 75 °C, 20,000 Pa, 9,600 ppm

after each dilution. Ten averaged spectra were recorded at each point, with the mean and standard deviation of each set being used for the corresponding point on the calibration curve. However, for acetic acid, the analyte volume mixing ratio was kept constant, and the total pressure varied, with spectra recorded at each pressure. This was due to the limited amount of time for which the certified acetic acid sample was available.

Prior to the acquisition of each spectrum, the CMR vessel was repeatedly purged to minimise the amount of atmospheric gases present. This involved evacuating the vessel for 5 min using a rotary pump, followed by backfilling with helium to approximately 80,000 Pa for a further 5 min. This was repeated three times, after which time the vessel was evacuated for a further 30 min. All of the certified gas mixtures used were supplied by BOC Ltd (UK) and consisted of: 10,000 ppm CO_2 in helium (certified 9,600 ppm), 1,000 ppm H_2O in helium (certified 1,090 ppm) and 1,000 ppm acetic acid in helium (certified 926 ppm).

All H_2O and CO_2 calibration spectra were recorded at or near 20,000 Pa and at 75 °C, which are typical conditions for our MMEs. The initial measurement generally related to the certified mixture in its undiluted form. To obtain lower concentration measurements, this was diluted in a stepwise fashion by adding helium (Grade A, BOC Ltd) to a pressure of 40,000 Pa, followed by evacuation back down to 20,000 Pa.

3 Results

Table 2 shows in detail the positions and identities of the ro-vibrational transitions used to detect and calibrate for H_2O and CO_2. The acetic acid analysis relied upon detection of the overtone of the hydroxyl stretch centred at 6,993 cm^{-1}, though as rotational resolution was not possible, the intensity of the vibrational band contour, in the region of the Q-branch, was monitored instead.

Figures 9, 10 11 show representative examples of the spectra obtained for each analyte, and the associated absorbance data derived from their analyses. The residuals shown for the H_2O, CO_2 and acetic acid have SDs (1σ) of 3.910×10^{-4}, 9.403×10^{-4} and 2.770×10^{-4}, respectively. Whilst the CO_2 spectrum is unremarkable, the H_2O spectrum shows contributions from both the water vapour inside the vessel, and the atmospheric water vapour within the temperature-controlled chamber. For CO_2, the low concentration present in the atmosphere (~400 ppm) was negligible, and so not observed in the spectrum. In a similar fashion, the acetic acid spectrum exhibits a contribution from atmospheric water vapour, in this case within the interferometer of the OSA. The water in the acetic acid spectrum should not prove problematic as it is readily distinguished from the acetic acid absorbance band. In contrast, care must be taken when analysing the H_2O spectra in order to ensure that the atmospheric and sample contributions are accurately deconvoluted. It is fortunate therefore

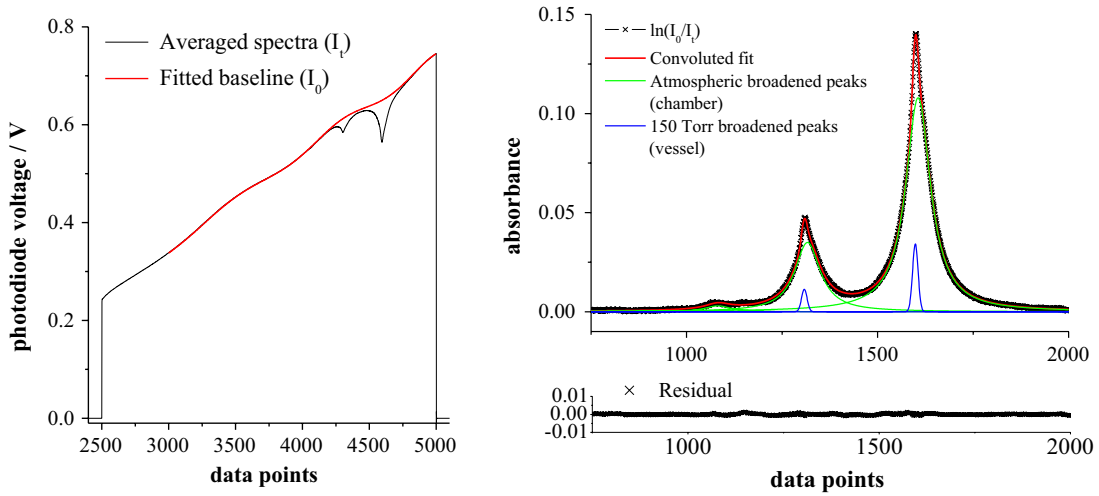

Fig. 10 A typical TDLAS spectrum and peak fit for H_2O in helium, 75 °C, 20,000 Pa, 1,090 ppm

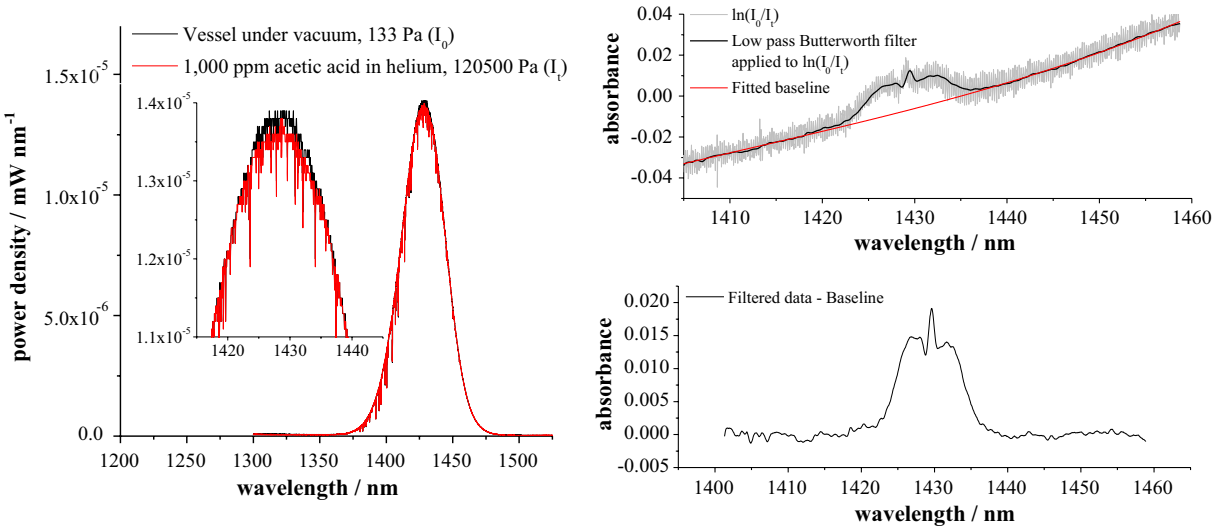

Fig. 11 A typical BBAS spectrum and filtering of acetic acid in helium, 75 °C, 120,500 Pa, 926 ppm

that the two contributions relate to H_2O at markedly different pressures, as this means that their line profiles will also be significantly different. A small pressure-based shift in the line centre (0.0018 nm) is also observed.

Figure 12 shows the results of the CO_2 calibration experiments. The data show excellent agreement ($R^2 = 0.99995$) with the Beer–Lambert law, and a limit of detection (based on a 3:1 signal-to-noise ratio) of 1,139 ppm m $Hz^{-0.5}$ ($\pm$41 ppm m $Hz^{-0.5}$) is obtained. SNR was calculated from the ratio of fitted absorbance peak height and three times the SD of the fit residual error.

Figure 13 shows the corresponding calibration trace for H_2O. In this case, the detection limit is 7 ppm m $Hz^{-0.5}$ ($\pm$22 ppm m $Hz^{-0.5}$), and the agreement with the Beer–Lambert law is again excellent ($R^2 = 0.99314$). The aforementioned requirement to deconvolute the atmospheric and low-pressure signals meant that it was necessary to approximate the atmospheric line profile with a Lorentzian function and the low-pressure profile with a Gaussian during the analysis process.

Finally, Fig. 14 shows the calibration data for acetic acid. Despite the fact that the various spectra were recorded at different pressures, and therefore, the effects of pressure broadening might be expected to cause some deviation, and the Beer–Lambert law appears to be adhered to ($R^2 = 0.9953$). A noise equivalent concentration of detection limit of 343 ppm m $Hz^{-0.5}$ ($\pm$40 ppm m $Hz^{-0.5}$), at 20,000 Pa pressure, serves to demonstrate that the combination of

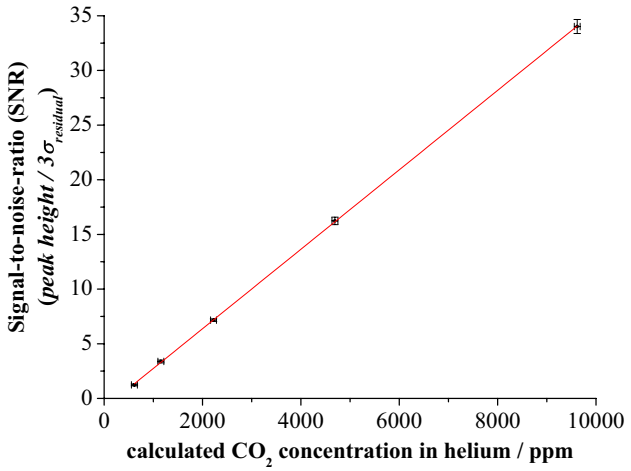

Fig. 12 Calibration graph of CO_2 in helium at 75 °C, 20,000 Pa over a 69 cm pathlength and 10 s averaging time (100 averages). *Error bars* correspond to one SD over ten measurements

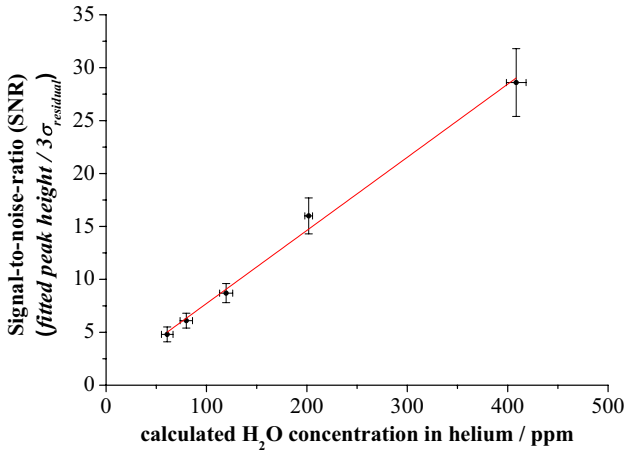

Fig. 13 Calibration graph of H_2O in helium at 75 °C, 20,000 Pa over a 69 cm pathlength and 10 s averaging time (100 averages). Error bars correspond to one SD over ten measurements

broadband source, CMR cell and OSA-based detection provides a viable method of obtaining quantitative data for this analyte. It should also be noted that acetic acid is almost uniquely problematic in this respect, as the variations in total pressure will cause changes in the equilibrium that exists in the vapour phase between hydrogen-bonded dimers and single, unbound molecules. Although this might have been expected to produce deviations from Beer–Lambert behaviour, significant deviations were not observed.

A common measure of noise and drift in spectroscopic systems can be assessed using an Allan–Werle deviation plot [13]. In order to estimate the Allan variance, the vessel was filled with the certified CO_2 gas mixture (9,600 ppm), to 20,000 Pa at 75 °C. Spectra were then recorded

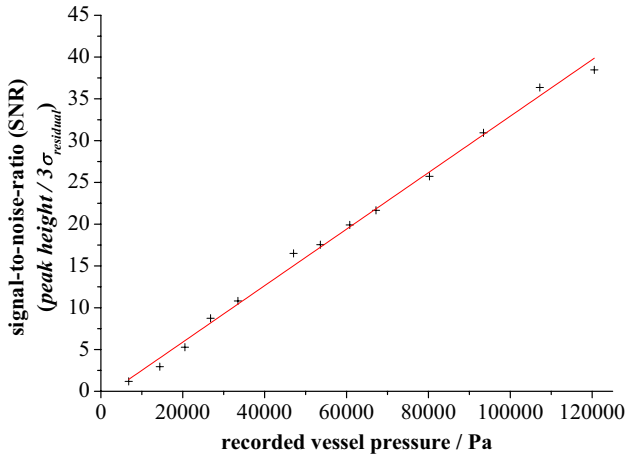

Fig. 14 Signal-to-noise ratio of 960 ppm acetic acid in helium as the total pressure is reduced, recorded at 75 °C

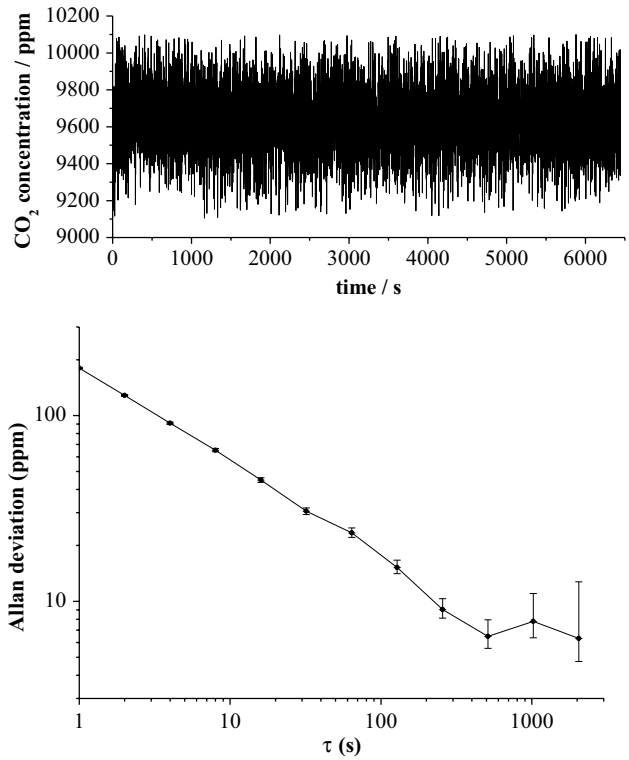

Fig. 15 (*upper*) Measured signal of CO_2 in helium with an integration time of 1 s (10 averages) for each data point. (*lower*) Allan–Werle deviation plot. 1-s averaging, measurement precision of 1.88 %

continuously for 2 h, where each spectrum comprised of 10 averages (integration time, $\tau = 1$ s), in contrast to the more usual 100 averages. An Allan–Werle deviation plot, shown in Fig. 15, was then generated using this CO_2 concentration data. The 1-s integration precision was found to be 1.88 %, which could be primarily attributed to the vibration associated with the fan of the temperature-controlled

chamber. Integrating for 512 s, however, resulted in a much improved precision of 0.07 %. It is assumed that a similar figure would be obtained for the other analytes, however, the significantly greater overheads associated with the data analysis for these species meant that the corresponding experiments have not yet been performed.

4 Discussion

Comparison of the available pathlength within the CMR cell with those reported by the various authors in Table 1 shows that our system did not achieve the expected optical pathlength for a cell of its size and design. The principal reason for this stems from errors in the mirror geometry introduced at the manufacturing stage. More specifically, several of the mirrors were found to have optical axes that were non-coincident with the axis of the component—i.e. their focal point was above or below the centre line of the mirror. The effect of this was that after a number of reflections, much of the infrared radiation was directed out of the plane of the CMR cell and lost. An additional effect of this inefficiency was to limit the available range of reflection geometries to a number of multi-point star patterns, all of which required the beam to repeatedly transit the cell at a significant distance from its centre point. This in turn introduced a significant astigmatism, further reducing the coupling efficiency of the output collimator. Investigations are currently ongoing into the procurement of improved mirrors that do not exhibit these deficiencies and a significant improvement in available pathlength, and hence, sensitivity is anticipated after their introduction. It is worth noting that a toroidal mirror design such as that used by Tuzson et al. [7] would impose limitations on our ability to vary pathlength, by changing reflection geometries and to maintain flexibility, a spherical design is preferred. Realistically, pathlengths of two to three metres should be attainable.

In respect of the detection limits obtained for the three analytes, perhaps most noteworthy is that for CO_2 (1,139 ppm m $Hz^{-0.5}$), which, when compared to that of H_2O, taking into account the difference in relative absorption cross sections (approximately 1:6, CO_2/H_2O) is seen to be higher than might be anticipated. The principal reason for this appears to be the amount of noise present in the CO_2 spectra. This mainly takes the form of a high-frequency interference pattern which is probably best attributed to back-reflections from optical components such as the collimators whose anti-reflection coating was optimised for ~1,500 nm and not ~2,000 nm. The thermal noise associated with the photoreceivers would also contribute to the enhanced noise figure. We have estimated the time-reduced minimum detectable absorption to be 2.82×10^{-3} $Hz^{-0.5}$. Future steps to reduce noise include improvements to the TDLAS control software, which is currently being upgraded to a smaller scan range to improve sensitivity. In addition, we look to increase the amount radiation collected from the vessel, as currently only 0.4 % of the input laser radiation reaches the detector. The main loss results from the small amount of light which falls on the variable collimating lens, which then must focus within the numeric aperture of the optical fibre.

A final area where revision or improvement may be possible concerns the nature of the temperature-controlled chamber. As mentioned earlier, vibrations from the fan of the chamber were transmitted to the vessel and caused a loss of precision which was only recovered by the use of longer integration times. Although the long integration times are not incompatible with materials ageing work, data from a typical materials trial could be collected on a daily or weekly frequency. An additional effect of these vibrations was a longer-term (weeks) drift in the alignment of the collimator/fibre assemblies. This would have more serious implications for materials ageing experiments which are typically conducted over extended periods, and interim realignments of the system would therefore be undesirable. Investigations into long-term system performance are currently ongoing.

5 Conclusions

Overall, the application of the CMR arrangement to the area of materials ageing trials in general and interfacial regions in particular appears to be a viable undertaking. The combination of CMR cell and ageing vessel described in this article shows acceptable sensitivity to the analytes of interest and also appears to satisfy other criteria such as stability and chemical inertness over short-to-medium timescales at least. The use of two different spectroscopic techniques shows that both lighter and heavier gases and vapours may be detected, and both cases in a quantitative manner. As always, further developments are possible, in this case the mirror quality being a particular area of interest. Notwithstanding such developments, the next stage of this work will involve the analysis of an interfacial region formed between material samples and the ageing products which accumulate therein, and in addition computational fluid dynamic (CFD) modelling of the system.

Acknowledgments Dr Albert Manninen (Empa, Switzerland) for his discussions regard CMR optics design, and Dr Paul Wynn (AWE plc) for his assistance and input into the CMR mirror holder design.

References

1. M. Patel, A.R. Skinner, Polym. Degrad. Stab. **73**, 399 (2001)
2. M.L. Thoma, R. Kaschow, F.J. Hindeland, Shock Waves **4**, 51 (1994)

3. M. Tonomura, H. Miyazawa, T. Nakamura, M. Endo, S. Yamaguchi, K. Nanri, T. Fujioka, in *Lasers and Electro-Optics, CLEO/Pacific Rim Conference* (2005)
4. Y. Kato, J. Sato, T. Nakamura, M. Endo, S. Yamaguchi, K. Nanril, T. Fujioka, in *Lasers and Electro-Optics, CLEO/Pacific Rim Conference* (2007)
5. J. Ofner, H.-U. Krüger, C. Zetzsch, Appl. Opt. **49**, 5001 (2010)
6. A. Manninen, B. Tuzson, H. Looser, Y. Bonetti, L. Emmenegger, Appl. Phys. B **109**, 461 (2012)
7. B. Tuzson, M. Mangold, H. Looser, A. Manninen, L. Emmenegger, Opt. Lett. **38**, 257 (2013)
8. P. Jouy, M. Mangold, B. Tuzson, L. Emmenegger, Y.-C. Chang, L. Hvozdara, H.P. Herzig, P. Wägli, A. Homsy, N.F. d Rooi, A. Wirthmueller, D. Hofstetter, H. Looser, J. Faist Anal. **139**, 2027 (2014)
9. J.U. White, J. Opt. Soc. Am. **32**, 285 (1942)
10. D. Herriott, H. Kogelnik, R. Kompfner, Appl. Opt. **3**, 523 (1964)
11. J.B. McManus, P.L. Kebabian, M.S. Zahniser, Appl. Opt. **34**, 3336 (1995)
12. L.S. Rothman, I.E. Gordon, A. Barbe, D.C. Benner, P.F. Bernath, M. Birk, V. Boudon, L.R. Brown, A. Campargue, J.-P. Champion, K. Chance, L.H. Coudert, V. Dana, V.M. Devi, S. Fally, J.-M. Flaud, R.R. Gamache, A. Goldman, D. Jacquemart, I. Kleiner, N. Lacome, W. Lafferty, J.-Y. Mandin, S.T. Massie, S.N. Mikhailenko, C.E. Miller, N. Moazzen-Ahmadi, O.V. Naumenko, A.V. Nikitin, J. Orphal, V.I. Perevalov, A. Perrin, A. Predoi-Cross, C.P. Rinsland, M. Rotger, M. Simeckova, M.A.H. Smith, K. Sung, S.A. Tashkun, J. Tennyson, R.A. Toth, A.C. Vandaele, J.V. Auwera, J. Quant. Spectrosc. Radiat. Transf. **110**, 533 (2009)
13. P. Werle, R. Mücke, F. Slemr, Appl. Phys. B **57**, 131 (1993)